Title
Determination of the depth-resolved Stokes parameters of light backscattered from turbid media by use of polarization-sensitive optical coherence tomography.

Journal
Optics letters, 24(5)

ISSN
0146-9592

Authors
de Boer, JF
Milner, TE
Nelson, JS

Publication Date
1999-03-01

DOI
10.1364/ol.24.000300

Determination of the depth-resolved Stokes parameters of light backscattered from turbid media by use of polarization-sensitive optical coherence tomography

Johannes F. de Boer

Beckman Laser Institute and Medical Clinic, University of California, Irvine, Irvine, California 92612

Thomas E. Milner

Biomedical Engineering Program, University of Texas at Austin, Austin, Texas 78712

J. Stuart Nelson

Beckman Laser Institute and Medical Clinic, University of California, Irvine, Irvine, California 92612

Received September 22, 1998

Polarization-sensitive optical coherence tomography (PS-OCT) was used to characterize completely the polarization state of light backscattered from turbid media. Using a low-coherence light source, one can determine the Stokes parameters of backscattered light as a function of optical path in turbid media. To demonstrate the application of this technique we determined the birefringence and the optical axis in fibrous tissue (rodent muscle) and *in vivo* rodent skin. PS-OCT has potentially useful applications in biomedical optics by imaging simultaneously the structural properties of turbid biological materials and their effects on the polarization state of backscattered light. This method may also find applications in material science for investigation of polarization properties (e.g., birefringence) in opaque media such as ceramics and crystals.

OCIS codes: 170.0170, 170.4500, 260.1440, 260.5430, 110.7050, 170.1870.

Optical coherence tomography (OCT) is emerging as an important technique in biomedical imaging.[1] In this Letter we present a new technique to determine the depth-resolved Stokes parameters of light backscattered from turbid media by use of polarization-sensitive optical coherence tomography (PS-OCT). Our instrument combines the principles of interferometric ellipsometry and OCT. Application of interferometry to characterize the polarization state of light was first demonstrated by Hazebroek and Holscher.[2] In their work, coherent detection of the interference fringe intensity in orthogonal polarization states formed by He–Ne laser light in a Michelson interferometer was used to determine the Stokes parameters of light reflected from a sample. Using a broadband source adds path-length discrimination to the technique. In previous work on PS-OCT,[3–6] incoherent detection techniques were used and were limited to measurement of two of the four Stokes parameters. In our instrumentation, coherent detection of the interference fringes in two orthogonal polarization states allows determination of the four Stokes parameters.

Both birefringence and scattering[6,7] can change the polarization state of light propagating in turbid media. When it is applied to biomedical optics, analysis of depth-resolved changes in the four Stokes parameters of light backscattered from biological tissues allows a better understanding and systematic analysis of the origin of polarization changes and corresponding structural properties. We demonstrate that the polarization changes in fibrous tissue can be attributed to birefringence and that in some tissues the optical axis can be determined when circularly polarized light is incident upon the sample. The orientation was verified by three measurements with linearly polarized light incident upon the tissue sample, with electric fields directed parallel, perpendicular, and at 45° to the measured optical axis. When it is applied to *in vivo* rodent skin with circularly polarized incident light, the variation with depth of the computed Stokes parameters demonstrates the presence of birefringence. Figure 1 shows a schematic of the PS-OCT system, which was described in detail in Ref. 8.

An algebraic expression for the depth-resolved Stokes parameters was derived in terms of the measured amplitude and the relative phase of the interference fringes in orthogonal polarization states. In our analysis the electric-field amplitude of each polarization component is represented by a complex analytic function,[9] $E(z) = \int \tilde{e}(k)\exp(-ikz)\,\mathrm{d}k$, with $k = 2\pi/\lambda$ and $\tilde{e}(k) = 0$ if $k < 0$. From the Wiener–Khinchine

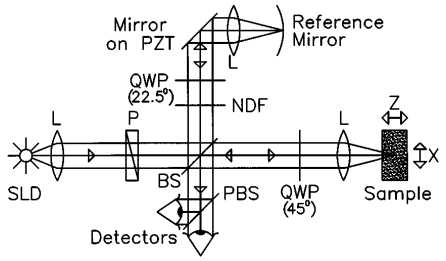

Fig. 1. Schematic of the PS-OCT system: SLD, superluminescent diode; L's, lenses; P, polarizer; BS, beam splitter; QWP's, quarter-wave plates; NDF, neutral-density filter; PBS, polarizing beam splitter; PZT, piezoelectric transducer.

0146-9592/99/050300-03$15.00/0

theorem, it follows that $\langle \tilde{e}^*(k)\tilde{e}(k')\rangle = S(k)\delta(k - k')$, which defines $\tilde{e}(k)$ in terms of the spectral density $S(k)$ of the source light, and the angle brackets denote ensemble averaging. Since light from the reference arm was split equally into horizontal and vertical polarization states with identical phase, the electric-field amplitude in the reference arm of the interferometer is given by

$$E_{x,y}(z_r) = \int_{-\infty}^{\infty} \tilde{e}(k)\exp(-2ikz_r)\,\mathrm{d}k\,, \tag{1}$$

where z_r is the length of the reference arm. The electric-field amplitude of light backscattered from the sample can be written as

$$\mathbf{E}(z_s) = \int_{-\infty}^{\infty} \sqrt{R(z_s)}\,\mathbf{a}(k, z_s)\tilde{e}(k)\exp(-2ikz_s)\,\mathrm{d}k\,, \tag{2}$$

where $\sqrt{R(z_s)}$ is a real number representing the reflectivity at depth z_s and the attenuation of the coherent beam by scattering and $\mathbf{a}(k, z_s)$ is a complex-valued Jones vector that characterizes the amplitude and phase of each polarization component of light with wave vector $\mathbf{k}$ that has backscattered from depth z_s, with $\mathbf{a}^*(k, z_s) \cdot \mathbf{a}(k, z_s) = 1$ and $\mathbf{a}(k, z_s) = 0$ if $k < 0$. Following the notation of Mandel and Wolf,[10] the Stokes parameters s_j with $j = 0, 1, 2, 3$ of the electric-field amplitude $\mathbf{E}(z_s)$ are

$$s_j(z_s) = \mathrm{tr}(\sigma_j \mathbf{J}) = R(z_s)\int [\mathbf{a}^*(k, z_s)\sigma_j \mathbf{a}(k, z_s)]S(k)\,\mathrm{d}k\,, \tag{3}$$

where $\mathbf{J}$ is the 2×2 coherency matrix[10]; $J_{k,l} = \langle E_k{}^* E_l\rangle$, where k and l take on the values x and y, respectively; σ_0 is the 2×2 identity matrix; and σ_1, σ_2, and σ_3 are the Pauli spin matrices. From Eqs. (1) and (2), the interference fringe intensity that was measured by the two detectors is given by

$$\begin{aligned} \boldsymbol{I}(z_s, \Delta z) &= 2\,\mathrm{Re}\begin{bmatrix} \langle E_x{}^*(z_r)E_x(z_s)\rangle \\ \langle E_y{}^*(z_r)E_y(z_s)\rangle \end{bmatrix} \\ &= \sqrt{R(z_s)}\int 2\,\mathrm{Re}[\mathbf{a}(k, z_s)\exp(-2ik\Delta z)] \\ &\quad \times S(k)\,\mathrm{d}k\,, \end{aligned} \tag{4}$$

with $\Delta z = z_s - z_r$. Retaining only the components for positive k of the Fourier transform of $\boldsymbol{I}(z_s, \Delta z)$ with respect to Δz gives the complex cross-spectral density function for each polarization component:

$$\boldsymbol{I}(z_s, 2k) = \frac{1}{2\pi}\sqrt{R(z_s)}\,\mathbf{a}(k, z_s)S(k) \text{ for } k \geq 0\,. \tag{5}$$

Using Eq. (5), we can express the Stokes parameters in Eq. (3) in terms of $I(z_s, 2k)$:

$$s_j(z_s) = (2\pi)^2 \int [\tilde{\boldsymbol{I}}^*(z_s, 2k)\sigma_j \tilde{\boldsymbol{I}}(z_s, 2k)]/S(k)\,\mathrm{d}k\,. \tag{6}$$

The Stokes parameters for each pixel were calculated according to Eq. (6) over Δz intervals of 10 μm, with the spectral density $S(k)$, estimated by $|\tilde{\boldsymbol{I}}(z_s, 2k)| = 1/(2\pi)\sqrt{R(z_s)}S(k)$. Because of this estimate of $S(k)$, $s_0(z_s)$ is related to the backscattered intensity summed over both polarization channels by $\langle|\boldsymbol{I}(z_s)|\rangle \propto \sqrt{R(z_s)}\,s_0(z_s)$. Unlike in previous work,[3–6] coherent detection of the interference fringe intensity for each polarization component allows determination of the additional Stokes parameters s_2 and s_3. To determine the polarization state of light backscattered from the sample (i.e., before the return pass through the QWP) we multiplied the Stokes vector by the inverse of the Mueller matrix associated with the QWP in the sample arm. OCT images of the Stokes parameters were formed by gray-scale coding of 20 log $s_0(z_s)$ over 35 or 40 dB and by gray-scale coding of the polarization-state parameters s_1, s_2, and s_3 normalized on the intensity s_0 from 1 to -1.

The Stokes parameters s_0, s_1, s_2, and s_3 were measured according to Eq. (6) in a laboratory frame defined by the orientation of horizontal and vertical polarization states of light exiting the polarizing cube in the detection arm of the interferometer. The Stokes parameters can also be presented in a sample frame with an orientation given by the axes of tissue birefringence. Orientation of the sample frame is determined by computation of the angle of rotation of the laboratory frame that minimizes the amplitude of oscillations with depth in s_1 or s_2 and gives the direction of the axes of tissue birefringence.

Rodent muscle was mounted in a chamber filled with saline solution and covered with a thin glass lip so that the muscle was not dehydrated during measurements. Figure 2 shows images of the four Stokes parameters in the sample frame for right-circularly polarized incident light. Several periods of s_2 and s_3, cycling back and forth between 1 and -1, are observed in muscle, as further demonstrated by the averages of the Stokes parameters over all depth profiles [Fig. 3(a)], indicating that the sample is birefringent. To verify experimentally the orientation of the optical axis we performed three measurements by replacing the QWP in the sample arm with a half-wave retarder. Light that was incident upon the sample was prepared in three linear polarization states with electric fields parallel, perpendicular, and at 45° to the experimentally determined optical axis of the birefringent muscle. Figure 3(b) shows the average of the Stokes parameter s_1 over all depth profiles at the same sample location. The negligible amplitude

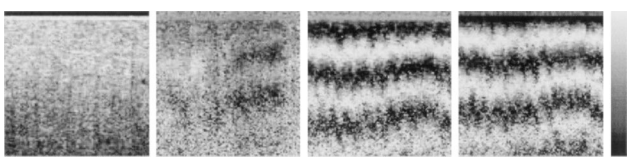

Fig. 2. PS-OCT images of *ex vivo* rodent muscle (1 mm × 1 mm; pixel size, 10 μm × 10 m). From left to right, the images show the Stokes parameters s_0, s_1, s_2, and s_3 in the sample frame for right-circularly polarized incident light. The gray scale to the right gives the magnitude of the signals, with a 35-dB range for s_0, and from 1 to -1 for s_1, s_2, and s_3.

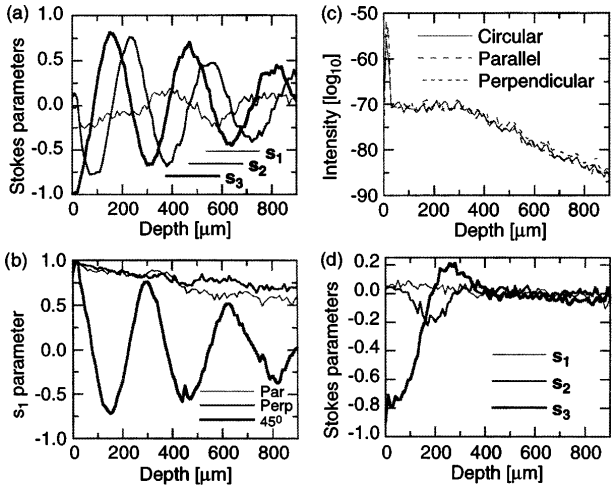

Fig. 3. Averages of Stokes parameters in the sample frame over all depth profiles of (a) rodent muscle, right-circular incident polarization; (b) rodent muscle, linear incident polarization parallel, perpendicular, and at 45° with the optical axis; (c) rodent muscle, right-circular, parallel, and perpendicular incident polarization; (d) *in vivo* rodent skin, right-circular incident polarization.

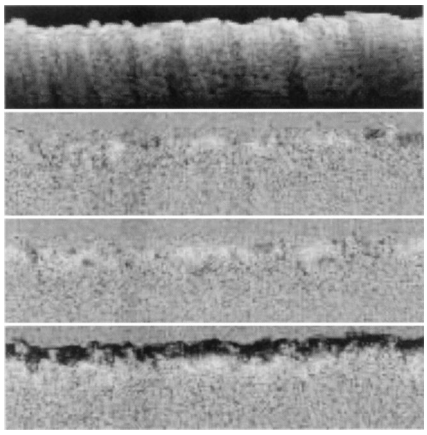

Fig. 4. PS-OCT images of *in vivo* rodent skin (5 mm × 1 mm; pixel size, 10 μm × 10 μm). From top to bottom, Stokes parameters s_0, s_1, s_2, and s_3 in the laboratory frame for right-circularly polarized incident light. The magnitude of signals ranged over 40 dB for s_0 and from 1 to −1 for s_1, s_2, and s_3.

of oscillation in s_1 for light polarized parallel and perpendicular to the optical axis verified the experimentally determined orientation. When light is incident at 45° to the optical axis of the sample, s_1 oscillates with increasing sample depth as expected for a birefringent sample. The similarity of the backscattered intensity for circular, parallel, and perpendicular light [Fig. 3(c)] indicates that the polarization state changes are not due primarily to the polarization dependence of the backscatter cross section of the muscle fibers. The birefringence δ was determined by measurement of the distance of a full s_3 period, which corresponds to a phase retardation of $\pi = k_0 z \delta$, giving $\delta = 1.4 \times 10^{-3}$.

Figure 4 shows PS-OCT images of the four Stokes parameters in the laboratory frame for right-circularly polarized light that was incident upon *in vivo* rodent skin. Averages of the Stokes parameters over all depth profiles [Fig. 3(d), after the oscillations in s_1 are minimized] indicate oscillations typical of sample birefringence in the first 400 μm. The observed birefringence is attributed to the presence of collagen in the skin. Although no preferred orientation of the optical axis is expected in rodent skin, a predominant direction was found at shallow depths. At deeper depths, s_1, s_2, and s_3 tend to zero, which is attributed to scrambling of the polarization by scattering and the randomly oriented and changing optical axis.

In conclusion, coherent detection of the interference fringe intensity in orthogonal polarization channels allows determination of the depth-resolved Stokes parameters in OCT. In a rodent muscle in which the optical axis was constant the birefringence and axes' orientations were determined. In rodent skin the observed oscillations in the Stokes parameters at superficial depths demonstrate that the tissue is birefringent. Because PS-OCT simultaneously gives structural information through the backscattered intensity and induced changes in the polarization, the technique may find useful applications in biomedical optics.

Research grants from the Institutes of Arthritis, Musculoskeletal and Skin Diseases and Heart, Lung, and Blood and the National Center for Research Resources of the National Institutes of Health, the U.S. Department of Energy, the U.S. Office of Naval Research, and the Beckman Laser Institute Endowment are gratefully acknowledged. J. F. de Boer's e-mail address is deboer@bli.uci.edu.

References

1. D. Huang, E. A. Sawnson, C. P. Lin, J. S. Schuman, W. G. Stinson, W. Chang, M. R. Hee, T. Flotte, K. Gregory, C. A. Puliafito, and J. G. Fujimoto, Science **254,** 1178 (1991).
2. H. F. Hazebroek and A. A. Holscher, J. Phys. E **6,** 822 (1973).
3. M. R. Hee, D. Huang, E. A. Swanson, and J. G. Fujimoto, J. Opt. Soc. Am. B **9,** 903 (1992).
4. J. F. de Boer, T. E. Milner, M. J. C. van Gemert, and J. S. Nelson, Opt. Lett. **22,** 934 (1997).
5. M. J. Everett, K. Schoenenberger, B. W. Colston, Jr., and L. B. Da Silva, Opt. Lett. **23,** 228 (1998).
6. J. M. Schmitt and S. H. Xiang, Opt. Lett. **23,** 1060 (1998).
7. M. I. Mishchenko and J. W. Hovenier, Opt. Lett. **20,** 1356 (1995).
8. J. F. de Boer, S. S. Srinivas, A. Malekafzali, Z. Chen, and J. S. Nelson, Opt. Express **3,** 212 (1998), http://epubs.osa.org/opticsexpress.
9. L. Mandel and E. Wolf, in *Optical Coherence and Quantum Optics* (Cambridge U. Press, Cambridge, 1995), Chap. 3.
10. Ref. 9, Chap. 6.